# Heat-Flux Measurements for the Rotor of a Full-Stage Turbine: Part II—Description of Analysis Technique and Typical Time-Resolved Measurements

M. G. Dunn
W. K. George
W. J. Rae
S. H. Woodward
J. C. Moller
P. J. Seymour

Calspan–UB Research Center,
Buffalo, NY 14225

*This paper presents a detailed description of an analysis technique and an application of this technique to obtain time-resolved heat flux for the blade of a Garrett TFE 731-2 hp full-stage rotating turbine. A shock tube is used as a short-duration source of heated air and platinum thin-film gages are used to obtain the heat-flux measurements. To obtain the heat-flux values from the thin-film gage temperature histories, a finite-difference procedure has been used to solve the heat equation, with variable thermal properties. The data acquisition and the data analysis procedures are described in detail and then their application is illustrated for three midspan locations on the blade. The selected locations are the geometric stagnation point, 32.7 percent wetted distance on the suction surface, and 85.5 percent wetted distance on the suction surface. For these measurements, the turbine was operating at the design flow function and very near 100 percent corrected speed. The vane–blade axial spacing was consistent with the engine operating configuration. The results demonstrate that the magnitude of the heat-flux fluctuation resulting from the vane–blade interaction is large by comparison with the time-averaged heat flux at all locations investigated. The magnitude of the fluctuation is greatest in the stagnation region and decreases with increasing wetted distance along the surface. A Fourier analysis by FFT of a portion of the heat-flux record illustrates that the dominant frequencies occur at the wake-cutting frequency and its harmonics.*

## Introduction

One of the basic turbomachinery problems that remains of interest concerns the unsteady flow environment generated as a result of rotating blades cutting through nozzle guide vane (NGV) wakes and the resulting influence of this unsteadiness on the blade surface-pressure and heat-flux distributions, on the inner blade-row gas-dynamic parameters, on the state of the boundary layer, and on the stage efficiency. Significant fluctuations in the local heat flux are important from a material fatigue or life cycle point of view. The specific component addressed in this paper is the turbine, but an early paper by Kerrebrock and Mikolajczak [1] addressing a similar problem for the compressor is very helpful in describing the essential physical processes that occur. Lakshminarayana et al. [2–4] have reported the results of several measurement programs designed to measure the boundary-layer and turbulence characteristics inside turbomachinery rotor passages using a large-scale slowly rotating rig as the test bed and hot-wire anemometry as the prime diagnostic. Dring et al. [5–7] have utilized a large-scale rotating rig which can be made to look like either a compressor or a turbine and with this facility they have performed many different types of measurements in the rotating frame including blade surface heat transfer and static pressure, total-pressure surveys and flow visualization. In [7], Dring et al. present the detailed results of a rotor–stator interaction study that included time-resolved thin-film gage data obtained on the blade. The authors demonstrate a strong unsteadiness near the blade leading edge that occurred at stator passing frequency. The magnitude of this fluctuation decreased with increasing distance away from the leading edge. They also found regions of large random fluctuation due to the turbulence in the stator wake that was superimposed on the periodic fluctuation.

Hodson [8–10] has utilized several different facilities to obtain measurements of wake-generated unsteadiness in the rotor passages and to perform measurements of boundary-layer transition and flow separation. In [9], detailed measurements of the unsteadiness contained in the rotor in-

Contributed by the Gas Turbine Division of THE AMERICAN SOCIETY OF MECHANICAL ENGINEERS and presented at the 31st International Gas Turbine Conference and Exhibit, Düsseldorf, Federal Republic of Germany, June 8–12, 1986. Manuscript received at ASME Headquarters January 13, 1986. Paper No. 86-GT-78.

flow are presented which illustrate the change in incidence angle and the change in turbulence associated with the stator wakes. The author does not present heat-flux data, but it is felt that both the change in incidence angle and the increased turbulence will influence the local blade heat transfer. Binder et al. [11] have looked at the influence of NGV wakes on the unsteady rotor flow using a laser velocimeter system. They illustrate very high turbuence levels associated with the stator wakes. The influence of this turbulence on the blade heat-flux level is not addressed. Doorly et al. [12, 13] have used a short-duration facility and a system of rotating bars to study the effects of shock waves and wakes shed by the NGV row on the turbine rotor flow field and surface heat-flux distribution. The authors have used thin-film heat flux gages to measure the magnitude of the heat-flux fluctuation experienced by a rotor blade in passing through the simulated wake. In [12] the authors present very nice Schlieren photographs illustrating the structure of the bar wake and its subsequent passage through the cascade. The technique is ideal for providing an environment in which detailed understanding of the flow phenomena associated with vane/blade interactions can be obtained.

The purpose of this paper is to present a detailed description of an analysis technique used to deduce time-resolved heat-flux data from thin-film heat-flux gages mounted on the rotor of a full-stage rotating turbine (Garrett TFE 731-2 hp). The long-range intent in this work is to spatially resolve the local heat flux to as small an area as possible and to perform these local measurements from the blade geometric stagnation point to near the blade trailing edge and to obtain the measurements in as realistic a turbine environment as is possible. Although a great deal of these data have been obtained as part of this program, it was felt that prior to presenting detailed time-resolved heat-flux data for the entire blade surface that have been obtained from such a complicated experiment, a thorough explanation of the data reduction procedures was in order. It should be kept in mind during this discussion that actual engine components (NGVs and blades) are used and they are not polished to a mirror finish. However, the heat transfer instrumentation is installed under a microscope and there is no surface discontinuity at the junction between the instrumentation and the component. The experimental technique being used is the short-duration, shock-tunnel approach, in which fast-response, thin-film thermometers are used to measure the surface temperature histories at prescribed locations on the blade. Instantaneous heat-flux rates can then be deduced from these temperature-time histories using a technique described herein. The shock-tunnel technique allows one to use actual turbine hardware and to operate it at the design flow function and at 100 percent corrected speed. Because of the high wake cutting frequency (approx. 13,000 wakes/s) and the short-duration ($\sim$ 20 to 30 ms) nature of this experimental technique, many new data-analysis techniques had to be developed in order to achieve the objectives. The rotor data of interest have been obtained and analyzed successfully using techniques that have not previously been applied to this problem and thus have not previously been published in this context.

The specific topics that will be addressed in this paper are: (*a*) description of the experimental technique, the heat-flux gage instrumentation, and the data recording procedure; (*b*) description of the analysis technique used to deduce the instantaneous heat-flux values from the gage surface-temperature histories; (*c*) description of the fast-Fourier transform analysis and associated data handling techniques that are used to obtain time-resolved data; and (*d*) application of the techniques that have been developed using rotor blade data obtained for a full-stage rotating turbine.

## Experimental Apparatus

The experimental apparatus used in this measurement program is described in detail in Part I of this paper and will not be repeated here. That portion of the apparatus and instrumentation new to this work will be described.

For the rotor speeds used here, a blade traverses a vane exit passage in approximately 75 $\mu$s. However, the blade traverses a vane wake in a significantly shorter time, on the order of 5 to 10 $\mu$s. In order to resolve vane wake cutting data and to avoid aliasing, it is important to be able to sample the thin-film gage output at a sampling rate of at least twice the highest frequency present in the signal (100 kHz in this experiment, requiring 200 kHz minimum sampling rate). In addition, one needs a minimum of 10 bit resolution and as much storage per channel as possible. Two different transient recorders, a Data Laboratories 2000 series and a Physical Data 515A, were used. Both of these were eight channel units with 4K words/channel storage capability and each channel could be sampled at a rate in the 200 kHz to 2 MHz range. Several other features of these units are particularly useful for obtaining time-resolved heat-flux data for a turbine stage: (*a*) The dual time base capability allows one to sample the early portion of a heat-flux gage history at a low sampling rate and then at a predetermined time to switch to a much higher sampling rate, (*b*) the multiple channel data stored in the recorder can be simultaneously displayed on an oscilloscope and photographed, (*c*) the stored data can be transferred to an on-line minicomputer (DEC LSI 11/23 plus) for additional analysis, printing, and plotting, and (*d*) the stored data can be transferred to tape and analyzed at a later date. A Sangamo Sabre III FM tape recorder with an 80 kHz bandwidth is normally used to record an additional 13 channels of high-frequency thin-film data. The majority of the data analysis is performed on a DEC VAX 11/780. A schematic of the on-line data recording system is given in Part I.

## Data Processing

The voltage output history from the thin-film gages and associated follower circuits shows typically a rapid rise in level ($\sim t^{1/2}$) with superimposed fluctuations. As noted earlier, a major objective of the present work has been to resolve quantitatively the time-dependent part of the heat transfer. Even though this part is generally greater than 10 percent of the time-averaged heat transfer rate, it is only a small fraction (typically 5 percent) of the temperature signal from the gages. Therefore, to resolve these fluctuations, it has been found necessary to revise some of the data-reduction procedures that have been used in the past.

The thin-film gage voltage output can be recorded digitally, or it can first be passed through an analog network [16, 17]. Both the analog and digital implementations have problems when applied to the gas turbine flow environment, especially when the heat-flux fluctuations are of interest. When either

## Nomenclature

$C$ = specific heat
$f$ = frequency, Hz
$j$ = $\sqrt{-1}$
$k$ = thermal conductivity
$n$ = quantization error
$S$ = spectrum
$t$ = time
$T$ = temperature
$x$ = distance normal to gage surface
$\alpha$ = thermal diffusivity = $k/\rho C$
$\eta, \tau$ = see equation (16)
$\rho$ = density
$\phi$ = see equation (15)
$\omega$ = radian frequency
$\hat{(\ )}$ = denotes Fourier transform

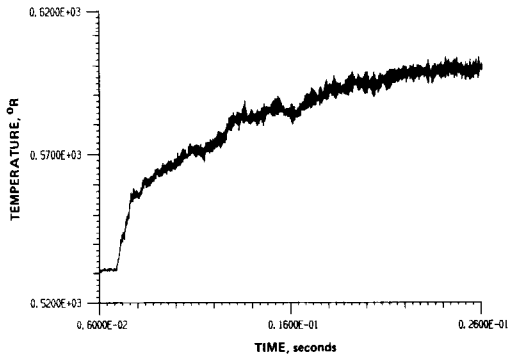


**Fig. 1(*a*) Surface temperature history at 32.7 percent wetted distance on blade suction surface**

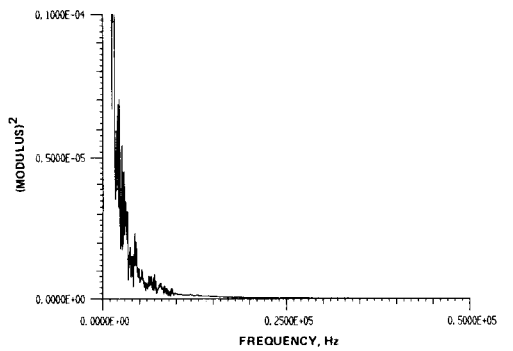


**Fig. 1(*b*) Modulus of Fourier transform of temperature history given in Fig. 1(*a*)**

temperature or analog outputs are sampled digitally, the subsequent analysis is limited by the quantization errors inherent in the A/D process. An additional problem arises from the fact that analog or Q-meter techniques depend on the assumption of the constant thermal properties of the substrate, an assumption not valid in the current environment. While computational algorithms can be devised which include variable thermal properties, numerical errors arising from the occurrence of a high-frequency skin depth preclude the use of such algorithms for the determination of fluctuating heat-flux values at frequencies approaching the sampling rate used here.

As part of this effort, a new approach to the problem has been developed. Surface temperature and its first derivative have been sampled digitally. From these a composite signal has been constructed which minimizes the effects of the quantization errors on the fluctuating signals. This composite temperature signal is then analyzed by a combination of numerical and Fourier transform techniques to yield a composite time-dependent heat-flux value. This high-fidelity signal is then available for subsequent analysis as will be described.

**Quantization Errors.** Quantization errors arise from the discretization of an analog signal. Whereas all values within a given range are possible for an analog signal, only those particular values corresponding to integral multiples of the step size are possible for a digitally sampled signal. Values of the signal between these discrete levels are simply placed into the nearest level. The sampled signal can thus be represented as the sum of the original signal and a random quantization error or noise.

The quantization noise can be modeled as being uncorrelated at different times and as having a uniform probability of being between $\pm\Delta/2$ where $\Delta$ is the step size of the A/D. (The step size can be determined by dividing the range of the A/D, say $R$, by the number of levels available. In our case the A/D was 10 bits so the number of levels was $2^{10} = 1024$, thus $\Delta = R/1024$.)

Figure 1(*a*) shows a typical surface temperature record from a thin-film gage on the suction surface of the blade (see Part I). The rapid rise in temperature signals the arrival of the test-gas flow and thus the initiation of the experiment. If this were the only phenomenon present, then heating the substrate would cause the surface temperature to rise as $T \sim t^{1/2}$ corresponding to a constant heat flux [19, 22]. As previously noted, it is this temperature rise over the course of the experiment which necessitates accounting for the variable thermal properties of the substrate on which the gage is painted.

The passage of the blade through the NGV wakes and the presence of turbulence and secondary flows in the NGV passage flow give rise to the fluctuations which are superimposed on the temperature history. If the unsteady heat-flux value is to be examined, it is these temperature fluctuations which must be faithfully translated into an unsteady heat-flux signal. Unfortunately, because the A/D converter must capture the entire range of temperature (since the instantaneous heat flux represents an integral over the temperature history), the fluctuating signal is discretized into only a small portion of the total voltage level available. As a consequence, *the unsteady signal of interest is likely to be buried in the quantization noise and the unsteady heat flux calculated from it will be primarily noise.*

The situation can best be illustrated by looking at the constant properties solution to the one-dimensional heat transfer equation

$$\rho C \frac{\partial T}{\partial t} = \frac{\partial}{\partial x}\left(k \frac{\partial T}{\partial x}\right) \tag{1}$$

subject to the surface boundary condition

$$q_w = -k \frac{\partial T}{\partial x}\bigg|_{x=0} \tag{2}$$

The objective is to relate the temperature at the surface to the heat flux there.

Let $\hat{q}_w(f)$ and $\hat{T}_w(f)$ be the Fourier-transformed heat flux and surface temperature defined by

$$\hat{q}_w(f) = \int_{-\infty}^{+\infty} e^{-j2\pi ft} q_w(t)\,dt \tag{3}$$

and

$$\hat{T}_w(f) = \int_{-\infty}^{+\infty} e^{-j2\pi ft} T_w(t)\,dt \tag{4}$$

Then it is straightforward to show that

$$\hat{q}_w(f) = \sqrt{j2\pi f}\,\sqrt{\rho Ck}\;\hat{T}_w(f) \tag{5}$$

or

$$|\hat{q}_w(f)| = \sqrt{\rho Ck}\,\sqrt{\pi f}\;|\hat{T}_w(f)| \tag{6}$$

and

$$\angle\,\hat{q}_w(f) = \angle\,\hat{T}_w(f) + \frac{\pi}{4} \tag{7}$$

where $\angle$ denotes the "phase angle of." Thus the modulus of the transform of the heat flux is proportional to the square root of the frequency times the modulus of the temperature, while the phase of the heat flux is the phase of the temperature shifted by +45 deg.

The exact manner in which quantization errors affect the calculation of heat flux from a quantized temperature will be the subject of a subsequent paper. The problem can be illustrated, however, by a simple example. Suppose that the unsteady heat flux due to a wake crossing corresponds to a square wave. Then the even harmonics are exactly zero, and the odd harmonics are related to the amplitude of the fundamental by $A_n/A_1 = 1/n$, where $(n-1)$ is the order of the

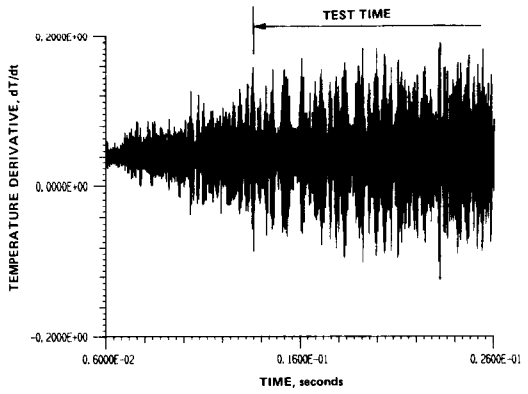


**Fig. 2(a) Temperature derivative signal at 32.7 percent wetted distance of blade suction surface**

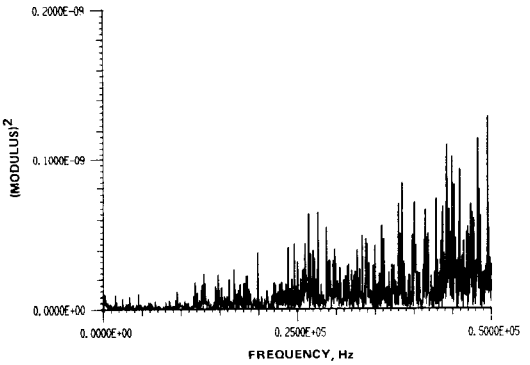


**Fig. 2(b) Modulus of Fourier transform on temperature derivative given in Fig. 2(a)**

harmonic. If the amplitude of the fundamental of the surface temperature sensed by the gage is $B_1$, then it follows from equation (6) that the odd harmonics are given by $B_n/B_1 = 1/n \cdot \sqrt{n}$. Thus if $B_1 \simeq 3$ R (as in Fig. 1), $B_3 \sim 0.55$ R, and $B_5 \leq 0.28$ R. If (as in Fig. 1), the range of the A/D is set to correspond to approximately 0 to 102.4 R and the number of bits of resolution is 10 corresponding to 1024 levels, the quantizing step size is 0.1 R. Thus the directly recorded temperature will have its harmonics largely obscured by the quantizing error. Because the effect of the quantization noise on the Fourier transform of the signal is random, the harmonics will be impossible to discern without substantial averaging of many independent experiments.

Figure 1(*b*) show the modulus squared of the Fourier transform of the temperature trace shown in Fig. 1(*a*). Clearly evident is the low-frequency portion of the signal associated with the overall rise in level. Not at all evident are the fundamental and harmonics of the wake crossing frequency which are buried in the random quantization noise (which is below the threshold of the plotter sensitivity). Since the fluctuating heat flux is proportional to the inverse transform of this signal multiplied by the square root of frequency and since the higher the frequency the weaker the Fourier components of the signal, the quantization noise dominates the calculated heat-flux transform as the frequency increases.

The statistics of the quantization noise can easily be computed if its probability density is known. Usually the quantization error is assumed to have a uniform probability of being between $\pm\Delta/2$. It follows that the mean square quantization error is $\Delta^2/12$. Most important for our application is that the spectrum of the quantization noise is white, that is, it is the same at all frequencies. Thus, if $S_n$ is noise spectrum as a function of the frequency $f$

$$S_n(f) = \begin{cases} (\Delta^2/12f_s & , \ f<f_s \\ (\quad 0 & , \ f>f_s \end{cases} \tag{8}$$

where $f_s$ is the sampling rate. The spectrum $S_n$ is calculated as

$$S_n(f) = \frac{1}{T}\overline{|\hat{u}_n(f)|^2} \tag{9}$$

where $T$ is the length in time of each individual record, $\hat{u}(f)$ is the Fourier transform of the noise for the record, and the overbar indicates that many realizations are averaged together.

In the data-analysis portions of this paper, plots of the modulus of the Fourier transform of signal plus noise are presented. It is important to note that although equations (8) and (9) imply that the mean square value of the Fourier transform of the noise is the same at all frequencies, transforms of individual records (unaveraged) will vary randomly from one frequency to another. Thus spurious peaks can appear in individual records which have no physical significance (certainly this is the case in Figs. 10–12). Nonetheless, it is clear from equation (8) that these random excursions are minimized by either decreasing the step size (less range or more bits) or by increasing the sampling rate.

The randomness of individual records is a characteristic of all random signals (such as turbulence) and is not unique to quantization noise. This randomness only disappears as successive independent records are averaged together. Thus care must be taken in inferring frequency content from individual records, and it should not be done unless there is a good physical reason to suspect that a particular frequency represents a nonrandom event. Such will be the case for the blade crossing harmonics identified later.

It is clear from the above that if fluctuating heat-flux rates are to be analyzed it is necessary to raise the fluctuating signal above the quantization noise *before* digitization. The analog Q-meter[1] accomplishes this by effectively multiplying the transform of the temperature by $\sqrt{j2\pi}\ f$ *before recording* so that the spectrum of the quantization noise (as it affects the heat flux) is now white instead of increasing linearly with frequency as in the directly recorded case. Another alternative that was used in this investigation is to differentiate the temperature before digitizing so that the transform of the digitized signal is $j2\pi f$ times that of the temperature. In this case the noise spectrum of the computed heat-flux signal will *roll off* linearly with frequency, thereby allowing even weaker signals to be captured at the higher frequencies.

Figure 2(*a*) shows the unsteady temperature derivative signal corresponding to Fig. 1(*a*). Gone is the rapid rise (since the low-frequency part of the signal has been buried in the noise by the multiplication of its transform by $j2\pi f$) while present in abundance are the high-frequency fluctuations which have been selectively and progressively amplified. In effect, the part of the signal corresponding to the unsteady flow has been spread over the entire range of the A/D so that the quantization errors are relatively much less. Figure 2(*b*) shows the Fourier transform of the derivative signal which clearly indicates how the higher frequencies have been raised above the quantization noise level.

**Composite Temperature.** While taking the derivative raises the fluctuations above the noise, it buries in the noise the overall temperature rise from which the varying thermal properties must be computed. In order to simultaneously capture both the overall rise and the unsteady characteristics with minimum quantization error, a hybrid scheme has been

[1] It was discovered in the course of this investigation that the Q-meters in common use [17], including ours, do not maintain the phase relation demanded by equation (7) over any of the frequency range of interest in this experiment (10 to 100 kHz). Therefore, the results obtained using the device are not reported here.

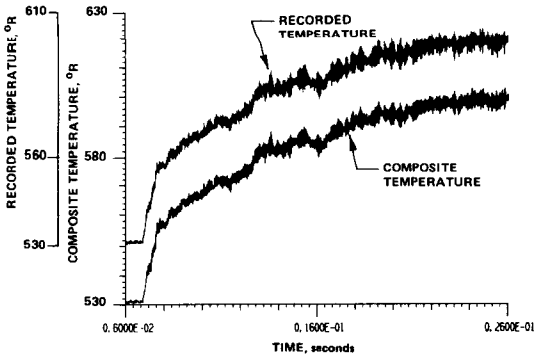


**Fig. 3(*a*) Comparison between temperature history as recorded and composite temperature history at 32.7 percent wetted distance on blade suction surface**

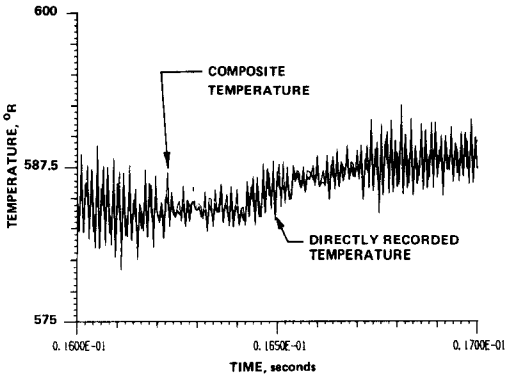


**Fig. 3(*b*) Comparison between directly recorded temperature and composite temperature in time interval 16 to 17 ms**

adopted which involves splicing two different signals in Fourier space. This is accomplished by simultaneously recording both the temperature and its derivative on separate channels. The recorded data are then Fourier transformed using a FFT alogrithm.

A minor complication arises from the fact that the records are of finite length. As a consequence, the transforms are not of the temperature and its derivative, but rather of the products of these functions with the time window $w(t)$ given by

$$w(t)=\begin{cases}1, & 0<t<t_1\\ 0, & \text{otherwise}\end{cases} \tag{10}$$

where $t_1$ is the record length. Thus

$$\hat{T}(f)=\int_{-\infty}^{+\infty} e^{-j2\pi ft}T(t)\quad w(t)dt \tag{11}$$

and

$$\hat{\dot{T}}(f)=\int_{-\infty}^{+\infty} e^{-j2\pi ft}\dot{T}(t)\quad w(t)dt \tag{12}$$

It is well known that if a signal of infinite length is sampled at a rate faster than twice the highest frequency present in the signal, the signal can be completely reconstructed [18] (this is the so-called Nyquist criterion). Moreover, the transforms of the signal and its first derivative differ by only a factor of $j2\pi f$. In our case, however, because of the window function which truncates the record, this is not true, even if the Nyquist criterion is satisfied. It is, however, straightforward to show for these finite length signals that the finite transforms of the recorded temperature and its derivative are related by

$$\hat{T}(f)=\frac{1}{j2\pi f}\{\hat{\dot{T}}(f)-[T(0)e^{j2\pi ft_1}-T(t_1)e^{-j2\pi ft_1}]\} \tag{13}$$

The term in brackets arises from the presence of the window function in the Fourier transform.

The composite temperature as a function of time has been assembled by carrying out the Fourier transform (using a FFT algorithm) on the composite transform defined by

$$\hat{T}_{\text{comp}}(f)=\begin{cases}\hat{T}(f), & f<f_1\\ \dfrac{1}{j2\pi f}[\hat{\dot{T}}(f)-(T(0)e^{j2\pi ft_1}-T(t_1)e^{-j2\pi ft_1})], & f>f_1\end{cases} \tag{14}$$

The frequency $f_1$ corresponds to the unity-gain frequency of the diffentiator and is chosen to be less than the primary wake crossing frequency, but greater than the frequencies comprising the overall temperature rise. In the experiments reported here, $f_1$ was approximately 10 kHz.

Figure 3 shows a comparison between the directly recorded temperature and the composite temperature computed from the inverse Fourier transform of equation (14). All subsequent references in the remainder of this paper to the temperature field and all calculations of heat flux presented will use the composite temperature field.

**Variable Thermal Properties.** The influence of variable substrate thermal properties on the deduced heat-flux value has been understood for a long time [19, 20], but until recently it has not been accounted for in data-reduction procedures [15]. The primary physical effect is an increase in the thermal conductivity of the substrate; thus a given heat-flux value produces a lower rise in surface temperature than would be produced by a substrate whose properties remain fixed at their pretest values. Conversely, the heat-flux value inferred from a given surface-temperature history is larger when variable thermal properties are accounted for. The error made by the constant-property model can be on the order of 5–15 percent [15], and is therefore not tolerable for the accuracy desired in the present work.

Consequently, the constant-property data-reduction procedures [19, 21, 16, 22] have been replaced in the present work by a finite-difference solution of equation (1), where it is convenient to employ the Kirchhoff transformation [23]

$$\phi\int_{T_{\text{ref}}}^{T}\frac{k}{k_{\text{ref}}}dT;\qquad \frac{\partial\phi}{\partial t}=\alpha\frac{\partial^2\phi}{\partial x^2} \tag{15}$$

In this equation $\alpha = k/\rho C$ is the temperature-dependent thermal diffusivity.

**High-Frequency Fluctuation of Surface Temperature.** For the problem of interest here, one must also be concerned with the high-frequency temperature fluctuations very near the gage surface. In [15], numerical solutions of equation (15) were reported, based on a Crank-Nicholson finite-difference procedure. The actual equation solved was a transformed version of equation (15), in which the $x$ coordinate was scaled by the thermal penetration depth

$$t=\tau,\qquad \eta=x/2\sqrt{\alpha_{\text{ref}}\,t} \tag{16}$$

In these variables, equation (15) is

$$\frac{\alpha}{\alpha_{\text{ref}}}\frac{\partial^2\phi}{\partial\eta^2}+\frac{2\eta\partial\phi}{\partial\eta}=4\tau\frac{\partial\phi}{\partial\tau} \tag{17}$$

This formulation has the advantage that the spatial scale is uniform in time. Numerical solutions using a fixed step size $\Delta\eta$ can then be found, for given values of $\phi$ at the surface, and for $\phi\to 0$ when $\eta$ is on the order of 3 to 5.

The above coordinate transformation is based on the assumption that the thermal penetration depth $\sqrt{\alpha t}$ is the significant length scale in the problem. Analytic solutions for the constant-property case reveal that this is the proper scale for a step-function time variation of the surface heat transfer.

However, when the heat transfer rate contains a part that fluctuates with frequency $\omega$, a second scale enters the problem, namely $\sqrt{\alpha/\omega}$, which is properly called the skin depth and is independent of time. The classical solution for a sinusoidal surface-temperature variation [23]

$$\Delta T_{\text{surface}}(t) = A\cos\omega t$$

contains an early-time transient plus the solution:

$$\Delta T(x,t) = A\exp\{-x\sqrt{\omega/2\alpha}\}\cos\{\omega t - x\sqrt{\omega/2\alpha}\} \quad (18)$$

Thus the high-frequency portion of the surface-temperature rise has a very shallow penetration, and care must be taken in the numerical work to resolve this thin layer properly. Solutions of equation (17) which use a fixed step size in the $\eta$-direction will have a small value of $\Delta x$ at early time, and a large one at late time. It has been found that for the blade-passing frequencies of interest here this procedure loses accuracy at late time. Accordingly, a revised procedure has been adopted, as described in the next paragraph.

Implicit numerical procedures for solving equation (17) work best when the step-size ratio

$$r \equiv \alpha\Delta t/(\Delta x)^2$$

is in the range 0.25 to 0.5. It happens that this criterion can be met for the test conditions of interest here. The sampling interval $\Delta t$ is taken, on the basis of the Nyquist criterion, to be inversely proportional to the highest frequency of interest

$$\Delta t \sim 1/\omega$$

The spatial step size $\Delta x$ must be small enough to resolve the skin depth; thus

$$\Delta x \sim \sqrt{\alpha/\omega}$$

Thus a constant value of the step-size ratio $r$ will satisfy both of these criteria.[2]

The finite-difference algorithm used is the simple implicit one:

$$\frac{\phi(i,j+1)-\phi(i,j)}{t_{j+1}-t_j} = \alpha(x_i,t_j) \times \frac{\phi(i+1,j+1)-2\phi(i,j+1)+\phi(i-1,j+1)}{(\Delta x)^2} \quad (19)$$

This equation was solved on a grid of variable size: At every time step, the boundary condition of zero temperature rise was enforced at a depth of $5\sqrt{\alpha_{\text{ref}}t}$. The heat transfer rate was found from a second-order-accurate expression for the derivative at the surface. As noted in (24), this algorithm is capable of following a rapidly fluctuating temperature more accurately than its Crank–Nicholson counterpart. However, numerical checks for a constant-property test case reveal that it does introduce a phase shift into the inferred heat transfer rate, and that accurate results require a time-step size small enough to give approximately 30 data points per cycle. (The test case used a heat-transfer rate consisting of a step function followed by a pure sine wave. The corresponding surface-temperature history contains a square root of time, plus a Fresnel-integral term that rapidly approaches a sine wave shifted by 45 deg.) In practice, because of memory limitations, the number of samples per cycle actually available from the A/D is usually much less then the 30 required; thus the numerical treatment decribed above is suitable only for the low-frequency portions of the recorded signal.

**Practical Scheme.** It is evident from the above that there is little hope of calculating by numerical techniques the heat-flux fluctuations at frequencies approaching the rate at which the data have been sampled. While it is theoretically possible for an infinitely long record (if the Nyquist criterion is satisfied) to upward decimate the data to as fine a time grid as desired, this is not true for a finite time record. Therefore, in principle, *no numerical technique will be able to produce a heat-flux history with the bandwidth of the originally recorded temperature signal.* If a sufficiently fast A/D with sufficient storage capacity were available, the problem could be easily solved by sampling the data at a much higher rate than needed. Unfortunately, the storage limitations of our hardware (4K/channel), the bandwidth of the experimental signals of interest (80–100 kHz), and the length of the test (20–30 ms), preclude this option. Fortunately, the nature of the signal itself provides an alternative.

It has already been pointed out that the temperature (and heat flux) events can be characterized by two different time scales: a slow time variation corresponding to the overall temperature rise, and a fast time variation corresponding to the gas dynamics associated with the rotating turbine. In fact, this dual nature of the signals has already been exploited in designing a recording scheme and in devising a computational grid. It will again be exploited here.

The scheme which has been adopted is based on the fact that it is the overall rise in temperature, or the *slow* process, which is primarily responsible for the variation in the thermal properties of the gage. The turbine gas dynamics, or *fast* process, is merely riding on the slow process. (Note that this would *not* be the case were the fluctuations due to the turbine of the same order of magnitude as the overall rise.)

It has already been shown that the frequency content of the overall rise is at frequencies substantially below the primary wake crossing rate in our experiments. Therefore, two new temperature signals can be created from the composite temperature defined earlier—a low-passed temperature, $T_{LP}(t)$, containing the slow process, and a high-passed temperature, $T_{HP}(t)$, containing the fast process. The heat flux associated with the low-passed temperature can then be analyzed by the variable property numerical technique described above, while the high-passed signal can be analyzed by applying the constant properties solution locally in time as described below.

The high- and low-passed temperature signals must be created by filtering the composite signal at any frequency below the wake crossing frequency subject to the following constraints:

(*i*) The low-passed signal must faithfully capture the overall rise, especially near the beginning of the experiment.

(*ii*) The sum of the high- and low-passed signals must equal the original temperature signal.

(*iii*) The filters must not introduce spurious oscillations or phase shifts in the time-series data.

Condition (*ii*) can be satisfied by any pair of linear filters. Condition (*iii*) eliminates the simple splitting in Fourier space used to develop the composite temperature since merely discarding the information above a given frequency corresponds to multiplying by a box-car window in frequency with the result that the low-passed signal oscillates badly in the time domain. Condition (*i*) can be determined by trial and error.

In our experiments, numerical RC-type filters were utilized with the following frequency response functions:

$$H_{LP}(f) = \frac{1}{1+jf/f_2} \quad (20)$$

$$H_{HP}(f) = \frac{jf/f_2}{1+jf/f_2} \quad (21)$$

A cutoff frequency $f_2$ of 2.5 kHz (about 1/5 the wake cross-

[2] The authors are grateful to Prof. Dale B. Taulbee, SUNY Buffalo, for calling attention to this fact and for suggesting use of the simple implicit method.

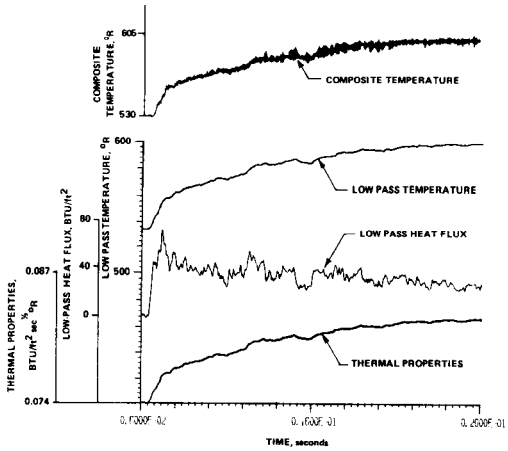


**Fig. 4 History of the composite temperature, low-pass temperature, the low-pass heat flux and the value of the variable thermal properties for 32.7 percent wetted distance on blade suction surface**

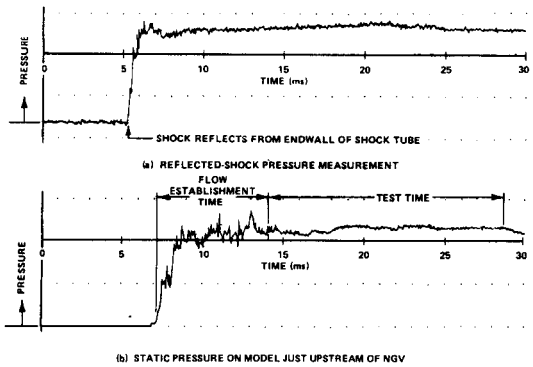


**Fig. 5 Typical shock tube reflected-shock pressure measurement and corresponding static pressure on turbine model upstream of NGV**

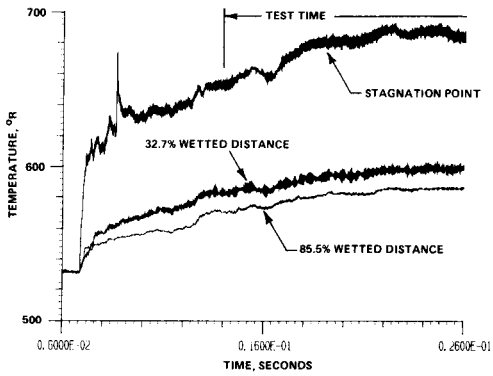


**Fig. 6 Composite temperature history at stagnation point, 32.7 percent wetted distance, and 85.5 percent wetted distance on blade suction surface**

ing rate) was found to adequately capture the initial rise (see Fig. 4).

The Fourier transforms of the low- and high-passed temperature signals are given by

$$\hat{T}_{LP}(f) = \hat{T}_{\text{comp}}(f)\, H_{LP}(f) \tag{22}$$

$$\hat{T}_{HP}(f) = \hat{T}_{\text{comp}}(f)\, H_{HP}(f) \tag{23}$$

The low-passed transformed composite temperature was then inverse transformed to yield $T_{LP}(t)$. This in turn was used as input to the variable properties numerical code described earlier to determine the low-passed heat-flux signal.

Figure 4 illustrates the composite and the low-passed temperature signals, and the heat flux and thermal properties history generated from the latter. Since the data were low-pass filtered at 2.5 kHz and sampled at 200 kHz, approximately 40 points/cycle were available to the numerical code at the frequency of the filter—well above any reasonable numerical requirements.

The heat flux from the high-passed temperature signal was computed directly from its Fourier transform using equation (5). Thus

$$\frac{1}{\sqrt{\rho Ck}}\,\hat{q}_{HP}(f) = \sqrt{j2\pi f}\,\hat{T}_{HP}(f) \tag{24}$$

from which the time-dependent high-passed heat flux (divided by $\sqrt{\rho Ck}$) can be obtained by inverse transformation. The actual time-dependent heat flux is computed by multiplying each time value so obtained by the local value of $\sqrt{\rho Ck}$ determined from $T_{LP}(t)$. This procedure can be formally justified by a two time scale expansion of equation (1). This technique has been utilized to obtain the results presented in the following section of the paper.

**Discussion of Results.** A description of the experimental conditions used in this work and a detailed discussion of the time-averaged heat-flux distributions for the blade surface is given in Part I of this paper. By way of a brief review, the flow conditions at the inlet to the NGV were: total temperature = 1000 R, static pressure = 98.5 psia, weight flow = 20.5 lb/s, turbulence intensity = 5.5 percent, and model wall temperature = 530 R. The turbine operates at 100 percent corrected speed with a rotor/stator axial spacing of 0.18 stator chord and a tip clearance of approximately 1.16 percent of blade height. The TFE 731 vane row operates with a throat Mach number on the order of 0.85. Therefore, the rotor gas dynamics should not be influenced by the presence of significant shock waves.

Previous publications [25, 26] have presented oscilloscope records and detailed discussions of pressure histories obtained at various locations within the model. However, a brief review of pressure records relevant to the heat-flux measurements described in this paper is appropriate. Figure 5 presents a typical shock tube reflected-shock pressure measurement and the corresponding static pressure on the bullet nose just upstream of the NGV row. The time at which the shock reflects from the shock tube endwall is noted on Fig. 5(*a*). As illustrated on Fig. 5(*a*), the pressure history of the reflected-shock reservoir that is supplying the air flow for the turbine model is very uniform for a substantial period of time. Figure 5(*b*) presents the corresponding static pressure obtained just upstream of the stator. The period of flow establishment is followed by the period of relatively uniform pressure called the test time. The results presented in Part I are the time-averaged heat-flux distributon over the test time shown in Fig. 5(*b*) while the results presented in this paper are obtained only up to about the 26 ms location on Fig. 5(*b*). In order to obtain the time-resolved data, the transient recorders discussed earlier must be used. These recorders have the disadvantage of limited storage (4K words/channel) but they have the advantages of high sampling rates and a dual time base. This dual time base can be used to sample the pretest base line and the flow establishment period at a relatively low frequency and then at a predetermined time, to initiate high-frequency sampling. Another alternative is to delay the initiation of sampling by a predetermined time selected on the basis of Fig. 5(*b*). Either of these techniques provides samples at constant time. However, an external clock driven by a shaft encoder has also been used in this work to sample at constant phase. Several shaft encoders were used in this work providing 1, 6, 41, 82, 500, and 1000 pulses per revolution. It is not possible

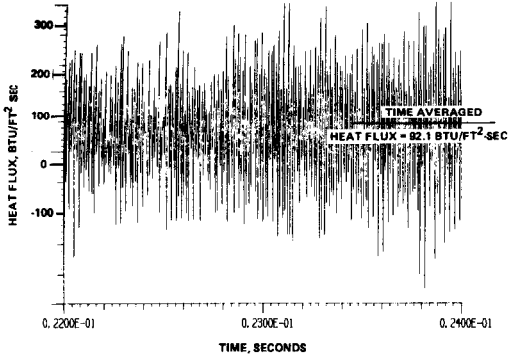


Fig. 7 Time-resolved heat-flux history at blade geometric stagnation point

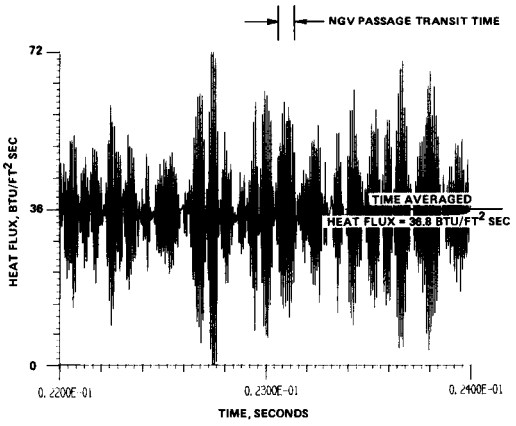


Fig. 8 Time-resolved heat-flux history at 32.7 percent wetted distance on blade suction surface

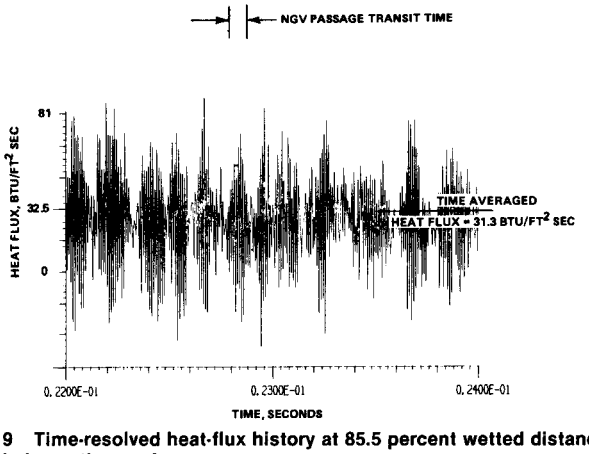


Fig. 9 Time-resolved heat-flux history at 85.5 percent wetted distance on blade suction surface

to discuss both data sets in this paper so the discussion will be confined to the data sampled at constant time.

Figure 6 presents the composite temperature histories for the geometric stagnation point, 32.7 percent wetted distance, and 85.5 percent wetted distance on the blade suction surface. The time at which uniform flow is established is denoted in Fig. 6. The maximum substrate temperature rise occurs in the stagnation region and it is in this region that the influence of variable thermal properties of the substrate becomes most important.

Figures 7–9 are the time-resolved heat-flux histories for the locations noted above computed in the manner described

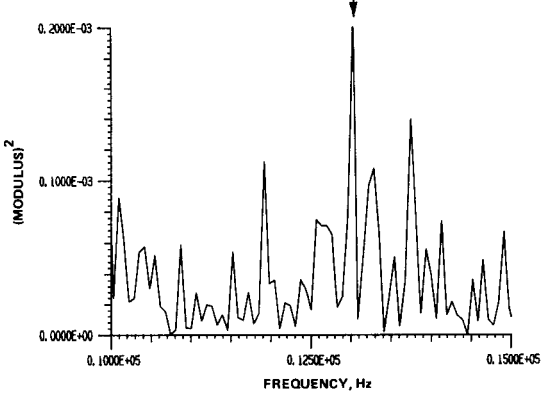


Fig. 10(a) Modulus of Fourier transform of heat-flux history for blade geometric stagnation point

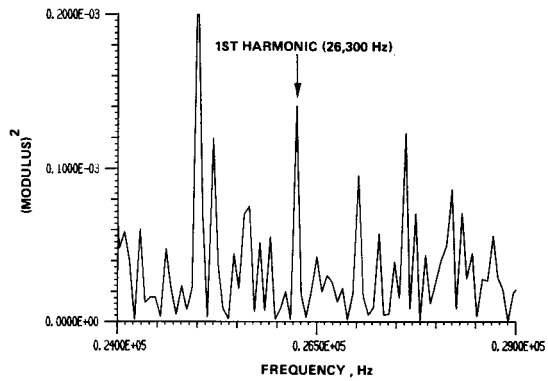


Fig. 10(b) Modulus of Fourier transform of heat-flux history for geometric stagnation point

earlier, for the time interval 22 to 24 ms. The time-averaged heat-flux value that is obtained from a separate data recording system and sampled at 20 kHz per channel is also shown on each of these plots. Figure 7 illustrates substantial fluctuations in the heat-flux value in the stagnation region. The magnitude of the fluctuation is time dependent as would be anticipated and a Fourier spectrum of the frequency content will be presented later in the paper. Moving back on the blade to the 32.7 percent location, the pattern of the heat-flux history is different as illustrated by Fig. 8. However, relative to the time-averaged heat-flux, the magnitude of the fluctuations is still significant at this location. Again, the value of the time-averaged heat flux is shown for comparison purposes. Figure 9 presents the heat-flux time history recorded near the trailing edge of the blade. The pattern at this location is similar to that observed elsewhere. Relative to the time-averaged heat flux, the fluctuations are significant even near the trailing edge of the blade.

The burst-like behavior observed in Figs. 7–9 is felt to be related to the period of the blade crossing the NGV exit passages. The characteristic time for the blade to traverse a single passage is denoted on each of the figures. In addition, the fluctuations of the calculated heat flux can be observed to go negative. The same features were observed when the temperature signal was directly input to a high-frequency Q-meter [17], and cannot, therefore, be readily attributed to the analysis. Thus it must either represent a phenomenon in the flow or be the effect of electronic noise.

Obviously, the heat-flux results given in Figs. 7–9 need to be analyzed further to determine whether or not the observed fluctuations are related to wake cutting. Figures 10–12 present the modulus squared of the Fourier transform, over a signifi-

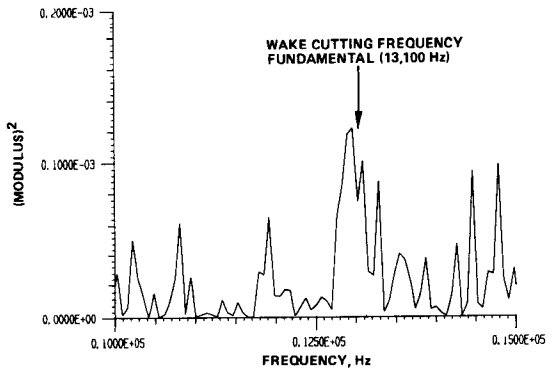


**Fig. 11(*a*) Modulus of Fourier transform of heat-flux history for 32.7 percent wetted distance on blade suction surface**

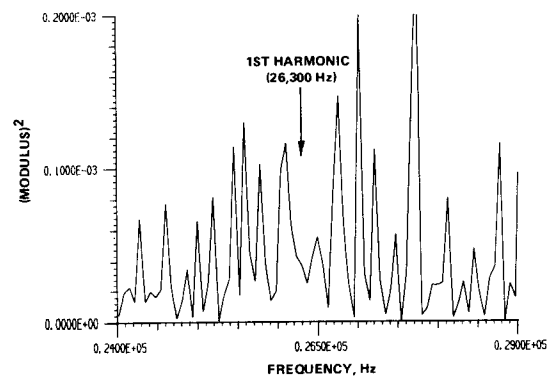


**Fig. 11(*b*) Modulus of Fourier transform of heat-flux history for 32.7 percent wetted distance on blade suction surface**

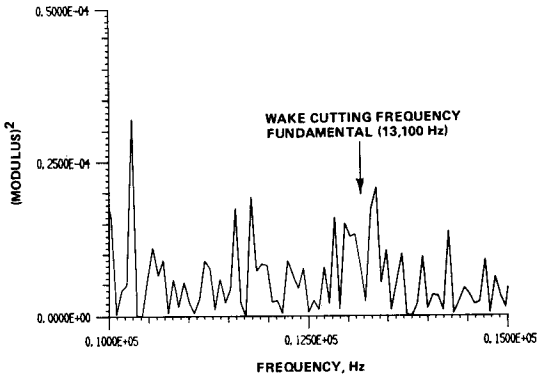


**Fig. 12(*a*) Modulus of Fourier transform of heat-flux history for 85.5 percent wetted distance on blade suction surface**

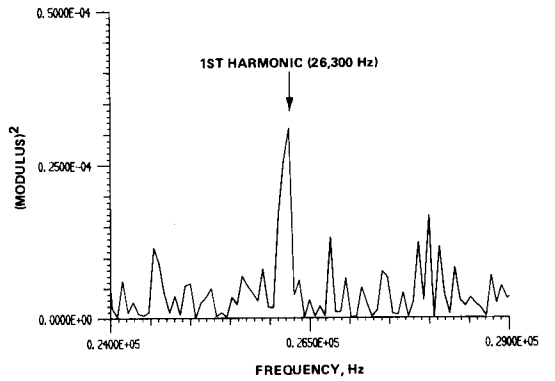


**Fig. 12(*b*) Modulus of Fourier transform of heat-flux history for 85.5 percent wetted distance on blade suction surface**

cant portion of the test time, of the heat-flux histories for the stagnation point, 32.7 percent, and 85.5 percent wetted distance, respectively. During this time period, the flow does work on the turbine, causing it to accelerate slightly. This acceleration has the effect of broadening the energy peaks associated with wake cutting. The frequency spectrum[3] is presented over a range of 10 to 15 kHz and 24 to 29 kHz. The previously mentioned shaft encoders were used to determine that the rotor speed at the 22 to 24 ms time interval was on the order of 19,200 rpm. For this turbine, there are 41 nozzle guide vanes and 78 rotor blades giving a fundamental wake cutting frequency of 13,100 Hz. Both the fundamental and the first harmonic are noted on Figs. 10–12.

The results for the stagnation region given on Figs. 10(*a*) and 10(*b*) demonstrate a sharp peak at the fundamental wake cutting frequency and two other rather broad peaks, of smaller magnitude, in the immediate vicinity. These later peaks suggest that there is significant energy content in the frequency range around the fundamental wake cutting frequency. The first harmonic peak at 26,300 Hz is shown on Fig. 10(*b*) as well as a relatively strong second peak at 25,000 Hz. At this time, it is not clear just what causes the 25 kHz peak.

Figures 11(*a*) and 11(*b*) present similar frequency spectra for 32.7 percent wetted distance on the suction surface. At this location, the FFT analysis suggests that the frequency content in the neighborhood of the fundamental has broadened, but is still very much related to wake cutting. The first harmonic at 26,300 Hz is very near a peak at 26,100 Hz and the previously observed peak at 25,000 Hz is reduced.

Figures 12(*a*) and 12(*b*) illustrate what one observes by moving farther along the surface toward the trailing edge. The frequency spectrum has a significant peak in the vicinity of the fundamental wake cutting frequency, but it is not as pronounced as at locations closer to the leading edge. The first harmonic, however, is very pronounced and stands out above all of the higher frequency content.

The results presented in Figs. 10–12 illustrate the presence of wake cutting in the heat-flux data. However, these frequency spectra also suggest that wake cutting is not the only important factor influencing blade heat transfer since there appears to be significant energy contained in other portions of the frequency domain.

## Conclusions

A description of an analysis technique and its application using typical data for time-resolved heat-flux measurements on the blade of a full-stage rotating turbine has been presented. The magnitude of the fluctuation is largest over the forward portion of the blade and decreases as the trailing edge is approached. However, relative to the time-averaged heat-flux values at this downstream location, the magnitude of the fluctuations is significant. An FFT analysis of the time-resolved heat flux demonstrates the presence of peaks at the fundamental and first harmonic of the wake cutting frequency. The frequency spectra also demonstrate the presence of energy at frequencies other than wake cutting.

## Acknowledgments

The research reported in this paper was supported by the National Aeronautics and Space Administration, Lewis Research Center, Cleveland, Ohio, under Grant No. NAG 3-469 and Grant No. NAG 3-581.

[3] The term "spectrum" is loosely used here to indicate the modulus squared of the Fourier transform of the record and no averaging is implied.

## References


1 Kerrebrock, J. L., and Mikolajczak, A. A., "Intra-stator Transport of Rotor Wakes and Its Effect on Compressor Performance," ASME JOURNAL OF ENGINEERING FOR POWER, Oct. 1970, pp. 359-368.

2 Gorton, C. A., and Lakshminarayana, B., "A Method of Measuring the Three-Dimensional Mean Flow and Turbulence Quantities Inside a Rotating Turbomachinery Passage," ASME JOURNAL OF ENGINEERING FOR POWER, Apr. 1976, pp. 137-146.

3 Amand, A. K., and Lakshminarayana, B., "An Experimental Study of Three-Dimensional Turbulent Boundary Layer and Turbulence Characteristics Inside a Turbomachinery Passage," ASME Paper No. 78-GT-114.

4 Lakshminarayana, B., Govindan, T. R., and Reynolds, B., "Effects of Rotation and Blade Incidence on Properties of Turbomachinery Rotor Wake," *AIAA Journal*, Vol. 20, No. 2, Feb. 1982, pp. 245-253.

5 Dring, R. P., and Joslyn, H. D., "Measurement of Turbine Rotor Blade Flows," ASME JOURNAL OF ENGINEERING FOR POWER, Apr. 1981, pp. 400-405.

6 Dring, R. P., Blair, M. F., and Joslyn, H. D., "An Experimental Investigation of Film Cooling on a Turbine Rotor Blade," ASME JOURNAL OF ENGINEERING FOR POWER, Jan. 1980, pp. 81-87.

7 Dring, R. P., Joslyn, H. D., Hardin, L. W., and Wagner, J. H., "Turbine Rotor-Stator Interaction," ASME JOURNAL OF ENGINEERING FOR POWER, Oct. 1982, pp. 729-742.

8 Hodson, H. P., "Boundary Layer and Loss Measurements on the Rotor of an Axial-Flow Turbine," ASME Paper No. 83-GT-4.

9 Hodson, H. P., "Measurements of Wake-Generated Unsteadiness in the Rotor Passages of Axial Flow Turbine," ASME Paper No. 84-GT-189.

10 Hodson, H. P., "Boundary-Layer Transition and Separation Near the Leading Edge of a High-Speed Turbine Blade," ASME Paper No. 84-GT-179.

11 Binder, A., Forster, W., Kruse, H., and Rogge, H., "An Experimental Investigation Into the Effect of Wakes on the Unsteady Turbine Rotor Flow," ASME Paper No. 84-GT-178.

12 Doorly, D. J., and Oldfield, M. L. G., "Simulation of the Effects of Shock Wave Passing on a Turbine Rotor Blade," ASME Paper No. 85-GT-112.

13 Doorly, D. J., Oldfield, M. L. G., and Scrivener, C. T. J., "Wake-Passing in a Turbine Rotor Cascade," *Heat Transfer and Cooling in Gas Turbines*, AGARD Conf. preprint No. 390, Bergen, Norway, May 6-10, 1985.

14 Dunn, M. G., and Holt, J. L., "Turbine Stage Heat Flux Measurements," AIAA/ASME 18th Joint Propulsion Conference, Cleveland, OH, June 21-23, 1982, Paper No. 82-1289.

15 Dunn, M. G., Rae, W. J., and Holt, J. L., "Measurement and Analysis of Heat-Flux Data in a Turbine Stage: Part I: Description of Experimental Apparatus and Data Analysis; Part II: Discussion of Results and Comparison With Predictions," ASME JOURNAL OF ENGINEERING FOR POWER, Vol. 106, Jan. 1984, pp. 229-240.

16 Skinner, G. T., "Analog Network to Convert Surface Temperature to Heat Flux," *Journal of the American Rocket Society*, June 1960, pp. 569-570.

17 Oldfield, M. L. G., Burd, H. J., and Doe, N. G., "Design of Wide-Bandwidth Analogue Circuits for Heat Transfer Instrumentation in Transient Tunnels," Oxford Univ., O.U.E.L. Report No. 1382/81.

18 Jenkins, G. M., and Watts, D. G., *Spectral Analysis and Its Application*, Holden-Day, San Francisco, 1968.

19 Vidal, R. J., "Model Instrumentation Techniques for Heat Transfer and Force Measurements in a Hypersonic Shock Tunnel," Cornell Aeronautical Laboratory Report M. AD-917-A-1, Feb. 1956.

20 Miller, C. G., "Comparison of Thin-Film Resistance Heat-Transfer Gages With Thin-Skin Transient Calorimeter Gages in Conventional Hypersonic Wind Tunnels," NASA TM 83197, 1981.

21 Cook, W. J., and Felderman, E. J., "Reduction of Data From Thin-Film Heat-Transfer Gages: A Concise Numerical Technique," *AIAA Journal*, Apr. 1966, pp. 561-562.

22 Schultz, D. L., and Jones, T. V., "Heat-Transfer Measurements in Short Duration Hypersonic Facilities," AGARDograph No. 165, Feb. 1973.

23 Carslaw, H. S., and Jaeger, J. C., *Conduction of Heat in Solids*, 2nd ed., Section 2.16, Clarendon Press, 1960.

24 Richtmeyer, R. C., and Morton, K. W., *Difference Methods for Initial Value Problems*, 2nd ed., Wiley, New York, 1967, Chap. 8.

25 Dunn, M. G., and Stoddard, F. J., "Application of Shock-Tube Technology to the Measurement of Heat-Transfer Rate to Gas Turbine Components," 11th International Symposium on Shock Tubes and Waves, July 1977.

26 Dunn, M. G., and Hause, A., "Measurement of Heat Flux and Pressure in a Turbine Stage," ASME JOURNAL OF ENGINEERING FOR POWER, Vol. 104, No. 1, Jan. 1982.